The response of an elastic-plastic clamped beam to transverse pressure loading

H.L. Gauch, F. Montomoli and V.L. Tagarielli*

Department of Aeronautics, Imperial College London, SW7 2AZ, UK

Abstract

This study presents a new analytical model to predict the response of elastic-plastic, fully clamped beams to transverse pressure loading. The model accounts for travelling elastic flexural waves, stationary and travelling plastic hinges, elastic-plastic stretching and plastic shear deformation. The predictions of the model are validated by detailed Finite Element simulations. The model is used to construct deformation mechanism maps and design charts.

Keywords: elastic-plastic beam, dynamic pressure load, plastic hinge, flexural wave, differential-algebraic equations.

Accepted in *International Journal of Impact Engineering*

* Corresponding author, Email: v.tagarielli@imperial.ac.uk

1 INTRODUCTION

The response of structures to dynamic loading has received considerable attention from researchers due to its relevance to several industrial applications. The presence of inertia force fields, nonlinear material behaviour, large deformations and failure render exact solutions inaccessible in most cases [1] and approximate methods are used to accurately predict deformation and failure in many cases [2].

The early work of Menkes and Opat [3] on fully clamped, impulsively loaded metallic beams experimentally identified three distinct failure modes, namely large inelastic deformation, tensile failure at the support, and transverse shear failure at the support. Many authors have attempted predictions of the failure loads associated with these mechanisms. The first analytical treatment of fully clamped beams subject to transverse pressure loading was given by Symonds [4], who simplified the problem by using a rigid perfectly-plastic material model and assuming small deflection. Jones [5] employed conservation of energy to develop an approximate solution for the deflection history of clamped beams made from rigid perfectly-plastic materials at large deformations. Subsequently, the same author [2],[6] presented accurate predictions of failure.

Fleck and Deshpande [7] improved the models of Symonds [4] and Jones [5] by including the effects of a travelling plastic hinge, for the case of an impulsively loaded beam undergoing large deformations. Shen and Jones [8] also modelled the effects of plastic shear deformation and employed an interactive yield criterion, successfully predicting the occurrence of different failure mechanisms. Yu and Chen [9] subsequently included the softening effect triggered by large plastic shear sliding upon the beam response, while Wen [10] investigated the influence of work hardening on the failure mechanisms.

The models presented above are accurate for the case of intense, diffused pressure loading of short time duration, typical of explosive blast events and neglect the influence of material elasticity on the response, which allows considerable simplification of the problem. Lee and Symonds [11] recognised that the ratio

$$R = \frac{\text{plastic work}}{\text{elastic energy capacity}} \tag{1}$$

has to take a value much larger than 1 for this assumption to be viable. It was found later that this condition is necessary, but not sufficient [12]. For the case of pressure loading of duration

comparable to the elastic response time of the structure, neglecting elasticity may lead to large errors. For example in combustion events, deflagration can induce on surrounding structures pressure loading of relatively low intensity (of order of a few bars) and large duration (of order 0.1 s) [13, 14], such that the assumption of rigid-plastic material response leads to inaccurate predictions; as a result, elastic-plastic models for dynamically loaded structures need to be developed.

Schleyer and Hsu [15] formulated predictions for beams subject to transverse pressure loading which included elastic effects; they assumed a deformation mode given by the superposition of two fundamental flexural mode shapes, neglecting transient flexural wave propagation, and only considered plasticity via concentrated elastic-plastic springs. More recent models [16] also included the influence of plastic shear and travelling plastic hinges, employing an interactive yield criterion as well as material softening; the initial elastic response of the beam, neglecting transient flexural wave propagation, was used to predict the onset of plasticity and the initial locations of plastic hinges; the subsequent motion of such hinges was assumed to be identical to that calculated in [8].

The role of the transient elastic response in dynamic loading of beams was studied in detail (e.g. [17]), while Yu et al. [18] showed, for the case of a cantilever, that the role of transient flexural waves is fundamental in determining the development of the plastic hinges and their location; on the other hand no published studies consider this aspect of the response in detail. In this study we present a new analytical model describing the elastic-plastic deformation of fully clamped beams; this accounts for an initial transient elastic response which allows predictions of the onset of yielding and of the initial location of plastic hinges; the subsequent structural response includes both elastic and plastic deformation and the motion of travelling plastic hinges is computed from Euler-Lagrange equations. The models account for large deformations and for the effects of elastic-plastic stretching and plastic shear upon the structural response. Due to its generality, the model is expected to be applicable to beams made from a wide range of materials and subject to diffuse pressure loading of arbitrary history.

The outline of the paper is as follows: the model is described in Section 2, while Section 3 presents details of the Finite Element (FE) simulations conducted. Results are presented and discussed in Section 4.

2 ANALYTICAL MODEL

2.1 Overview

The proposed model aims at capturing the response of a clamped beam from quasi-static to intense dynamic loading. The structural response is divided into several different phases and equations of motion are derived for each of these phases; these take the form of ordinary differential equations (ODEs) with algebraic constraints and are integrated numerically in non-dimensional form.

The problem investigated is defined in Fig. 1. A fully clamped beam of length 2*L* is loaded by a uniformly distributed transverse pressure *p(t)*. The beam's cross section is rectangular of height *H* and width *B* and is made of an isotropic, elastic-perfectly plastic material with Young's modulus *E*, yield stress σ_y and density ρ. Only half of the beam is analysed due to symmetry, such that $x = 0$ corresponds to a support section (Fig. 1).

Based on FE predictions conducted in this study (and described below) or published by other authors [2, 8, 19], the response of the beam is idealised as sketched in Fig. 2; in all phases it is assumed that only transverse displacements are present. The elastic longitudinal waves are neglected, as they propagate at sonic speed (of order $5000\ \mathrm{ms}^{-1}$ in steel), and consequently the axial stress in the beam is taken as uniform over the length. In all phases of the response the shape of the deflected profile of the beam is approximated by a polynomial of order four.

In all phases of the response the internal loads are described by the generalised stresses

$$M = \int_A \sigma_x z \mathrm{d}A, \quad N = \int_A \sigma_x \mathrm{d}A, \quad Q = \int_A \sigma_{yz} \mathrm{d}A, \tag{2}$$

where *A* is the beam's cross section area; these are referred to as bending moment *M*, membrane force *N* and shear force *Q*. The transition to plasticity is described by an interactive yield criterion (as in e.g. [8]); this has the form

$$\left|\frac{M}{M_0}\right| \sqrt{1 - \left(\frac{Q}{Q_0}\right)^2} + \left(\frac{Q}{Q_0}\right)^2 + \left(\frac{N}{N_0}\right)^2 = 1 \tag{3}$$

$$M_0 = \frac{BH^2\sigma_y}{4}, \quad Q_0 = \frac{BH\sigma_y}{\sqrt{3}}, \quad N_0 = BH\sigma_y. \tag{4}$$

Subsequent to first yield, an associated flow rule (normality) is assumed to determine the plastic strain increments.

If the condition (3) is met at any cross-section, it is assumed that a plastic hinge develops at this cross-section. Additional degrees of freedom (dofs) are added to the model to describe plastic dissipation at the hinge location; for plastic hinges at the supports, three dofs are introduced (namely, plastic hinge rotation $\theta_{\mathrm{pl,sup}}$, plastic shear displacement $w_{\mathrm{pl,sup}}$ and plastic axial stretching $\Delta l_{\mathrm{pl,sup}}$), while for plastic hinges along the beam span two additional dofs are included (plastic hinge rotation $\theta_{\mathrm{pl,mid}}$ and plastic axial stretching $\Delta l_{\mathrm{pl,mid}}$).

The response begins with an elastic phase (Phase I) involving the propagation of a flexural wave from the support towards mid-span. In this phase the deformation of the beam is described by two degrees of freedom, namely the mid-span deflection w_0 and the position of the flexural wave front ξ, as in Schiffer et. al [19].

As sketched in Fig. 2, Phase I is followed by either Phase IIa, corresponding to the flexural wave reaching mid-span, or Phase IIb, corresponding to yielding at the supports. In Phase IIa the propagation of the transient flexural wave is assumed to cease and the response is described by a single degree of freedom (the mid-span deflection w_0). With further deflection, the generalised stresses at the supports may become sufficiently high to cause plasticity; in this case, a plastic hinge is formed at the supports and the corresponding response is denoted as Phase IIIa.

In Phase IIb the elastic flexural wave motion continues and a plastic hinge develops at the support, inducing energy dissipation. Subsequently, a second plastic hinge may form along the beam at the flexural wave front ($x = \xi$), and the corresponding response is denoted as Phase IIIb; such second hinge is assumed to travel towards mid-span and its location is taken as coincident with the wave front of the elastic flexural wave ($x = \xi(t)$). During Phase IIIb the plastic deformation at the support may cease, and the corresponding phase is denoted as Phase IIIb2.

Phase IV corresponds to formation of stationary hinges at the supports as well as mid-span. This phase can be reached in three different ways: (i) after Phase IIIa, when the mid-span section yields with continued deformation; (ii) after Phase IIIb, when the travelling plastic hinge reaches mid-span ($\xi = L$); (iii) after Phase IIIb2, as the travelling plastic hinge reaches mid-span (corresponding to Phase IV2 in Fig. 2) and subsequently plastic deformation resumes at the supports.

Phase V denotes elastic rebound. This phase can reached from Phase IIIa, Phase IV or Phase IV2 when plastic deformation ceases. If pressure is still applied in the elastic rebound phase, the response of the beam can revert to either Phase IIIa or Phase IV2.

2.2 Governing equations

In this section we develop the governing equations for the individual phases of the response. In each phase we postulate the deformed shape of the beam, reducing the problem to a finite small number of dofs; then, the Euler-Lagrange equations (e.g. [20]) are used to deduce the equations of motion. Constraints arising from the yield criterion and the associated flow rule are treated via Lagrange's multiplier method.

2.2.1 Response in presence of elastic flexural wave or travelling plastic hinges

This first type of response refers to phases I, IIb, IIIb and IIIb2 in Fig. 2, involving propagation of an elastic flexural wave or a travelling plastic hinge, at location $x = \xi$. The elastic response of the beam is described by Rayleigh beam theory, accounting for the rotary inertia of the beam. The deflected shape of the beam for $0 \le x \le \xi$ is modelled as a fourth-order polynomial, whose coefficients are determined by imposing by imposing the boundary conditions

$$\begin{aligned} &w(x=0) = w_{\text{pl,sup}}, \qquad \frac{\partial w}{\partial x}(x=0) = \theta_{\text{pl,sup}}, \qquad w(x=\xi) = w_0, \\ &\frac{\partial w}{\partial x}(x=\xi) = 0, \qquad \frac{\partial^3 w}{\partial x^3}(x=\xi) = 0, \end{aligned} \tag{5}$$

where $w_{\text{pl,sup}}$ and $\theta_{\text{pl,sup}}$ vanish for the case of a purely elastic response. The portion $\xi \le x \le L$ is taken as undeformed, as sketched in Fig. 3. The resulting shape function reads

$$w(x,t)=\begin{cases} w_{\mathrm{pl,sup}}(t)+x\theta_{\mathrm{pl,sup}}(t)-\dfrac{x^2}{2\xi^2}(8w_{\mathrm{pl,sup}}(t)-8w_0(t)+5\theta_{\mathrm{pl,sup}}(t)\xi(t))+ \\ +\left(\dfrac{2x^3}{\xi^3}-\dfrac{x^4}{2\xi^4}\right)(2w_{\mathrm{pl,sup}}(t)-2w_0(t)+\theta_{\mathrm{pl,sup}}(t)\xi(t)) \quad \text{for } 0\le x\le\xi, \\ w_0(t) \quad \text{for } \xi < x \le L. \end{cases} \tag{6}$$

Neglecting elastic shear deformation, the curvature of the beam can be expressed as

$$\kappa=\frac{\partial^2 w}{\partial x^2} \tag{7}$$

and the elastic membrane strain is calculated as

$$\begin{aligned} \varepsilon_{\mathrm{el}} &\approx \frac{\Delta l-\Delta l_{\mathrm{pl}}}{L}=\frac{1}{L}\left(\int_0^L\sqrt{1+\left(\frac{\partial w}{\partial x}\right)^2}\,\mathrm{d}x-L-\Delta l_{\mathrm{pl}}\right) \\ &\approx \frac{1}{L}\left(\int_0^L\frac{1}{2}\left(\frac{\partial w}{\partial x}\right)^2\mathrm{d}x-\Delta l_{\mathrm{pl,sup}}-\Delta l_{\mathrm{pl,mid}}\right) \end{aligned} \tag{8}$$

where the plastic stretching $\Delta l_{\mathrm{pl,sup}}$ and $\Delta l_{\mathrm{pl,mid}}$ are absent for a perfectly elastic response. The generalised stresses can be expressed as

$$M=-EI_y\kappa, \qquad N=EBH\varepsilon_{\mathrm{el}}, \qquad Q=\frac{\partial M}{\partial x}+\rho I_y\frac{d^2}{dt^2}\left(\frac{\partial w}{\partial x}\right), \tag{9}$$

where $I_y=BH^3/12$ denotes the second moment of area with respect to the y-axis. The kinetic and potential energy follow as

$$\begin{aligned} T &= \frac{1}{2}\int_0^L\rho BH\dot{w}^2\mathrm{d}x+\frac{1}{2}\int_0^L\rho I_y\left(\frac{d}{dt}\left(\frac{\partial w}{\partial x}\right)\right)^2\mathrm{d}x \\ V &= \frac{1}{2}\int_0^L EI_y\kappa^2\mathrm{d}x+\frac{1}{2}\int_0^L EBH\varepsilon_{\mathrm{el}}^2\mathrm{d}x. \end{aligned} \tag{10}$$

and the Lagrangian can be calculated $L=T-V$. We note on passing that the maximum elastic strain energy which can be stored in the beam is given by

$$V_{\max}=\frac{1}{2}EBH\int_0^L\varepsilon_y^2dx=\frac{BHL\sigma_y^2}{2E}. \tag{11}$$

When the yield criterion is met at a certain cross-section, further plastic straining is computed employing the yield condition (3) and the assumption of an associated flow rule [2]. This introduce both holonomic and non-holonomic constraints. In the case of a stationary plastic hinge at the supports (subscript ‘sup’) the constraints read

$$f_{\text{sup}} = \left| \frac{M_{\text{sup}}}{M_0} \right| \sqrt{1 - \left(\frac{Q_{\text{sup}}}{Q_0} \right)^2} + \left(\frac{Q_{\text{sup}}}{Q_0} \right)^2 + \left(\frac{N}{N_0} \right)^2 - 1 = 0 \tag{12}$$

$$\frac{M_0}{\frac{\partial f_{\text{sup}}}{\partial \frac{M_{\text{sup}}}{M_0}}} \dot{\theta}_{\text{pl,sup}} - \frac{Q_0}{\frac{\partial f_{\text{sup}}}{\partial \frac{Q_{\text{sup}}}{Q_0}}} \dot{w}_{\text{pl,sup}} = 0 \ , \tag{13}$$

$$\frac{N_0}{\frac{\partial f_{\text{sup}}}{\partial \frac{N}{N_0}}} \Delta \dot{l}_{\text{pl,sup}} - \frac{M_0}{\frac{\partial f_{\text{sup}}}{\partial \frac{M_{\text{sup}}}{M_0}}} \dot{\theta}_{\text{pl,sup}} = 0 \ . \tag{14}$$

If a travelling plastic hinge forms along the beam at $x = \xi$ (subscript 'mid'), it is assumed that localised plastic shear sliding is absent ($w_{\text{pl,mid}} = 0$); as shear forces vanish at this location, the constraints read

$$f_{\text{mid}} = \left| \frac{M_{\text{mid}}}{M_0} \right| + \left(\frac{N}{N_0} \right)^2 - 1 = 0 \ , \tag{15}$$

$$\frac{N_0}{\frac{\partial f_{\text{mid}}}{\partial \frac{N}{N_0}}} \Delta \dot{l}_{\text{pl,mid}} - \frac{M_0}{\frac{\partial f_{\text{mid}}}{\partial \frac{M_{\text{sup}}}{M_0}}} \dot{\theta}_{\text{pl,mid}} = 0 \ . \tag{16}$$

The Lagrange multiplier method (e.g [21]) is used to implement the n holonomic and m non-holonomic constraints as

$$\frac{\mathrm{d}}{\mathrm{d}t} \frac{\partial L}{\partial \dot{q}_i} - \frac{\partial L}{\partial q_i} = Q_{\text{ext},i} + Q_{\text{diss},i} + \sum_{j=1}^{n} \lambda_{\text{h},j} \frac{\partial f_j}{\partial q_i} + \sum_{k=1}^{m} \lambda_{\text{nh},k} A_{ki} \ . \tag{17}$$

In eq. (17), $\mathbf{q}$ denotes the vector of generalised coordinates

$$\mathbf{q} = \left[w_0, \xi, \theta_{\text{pl,sup}}, w_{\text{pl,sup}}, \Delta l_{\text{pl,sup}}, \Delta l_{\text{pl,mid}} \right]^{\mathrm{T}} , \tag{18}$$

$Q_{\text{ext},i}$ and $Q_{\text{diss},i}$ describe the non-conservative generalised forces resulting from external load and plastic dissipation, respectively. The parameter $\dot{\theta}_{\text{pl,mid}}$ is computed as

$$\dot{\theta}_{\text{pl,mid}} \approx \frac{\mathrm{d}}{\mathrm{d}t} \frac{\partial w}{\partial x} (x = \xi) \ . \tag{19}$$

The constraint forces on the right hand side of equation (17) result from the holonomic constraints (12) and (15), of form

$$f_j(q_i) = 0 \tag{20}$$

and use the Lagrange multipliers $\lambda_{\mathrm{h},j}$. The non-holonomic constraints (13),(14) and (16) can be written in the general form

$$A_{ki}(q_i)\dot{q}_i = 0 \tag{21}$$

and are associated to the Lagrange multipliers $\lambda_{\mathrm{nh},k}$.

The virtual work done by the external load $p(t)$ gives rise to the generalised forces $Q_{\mathrm{ext},i}$

$$\delta W_{\mathrm{ext}} = \int_0^L pB\,\delta w\,\mathrm{d}x = \sum_i \int_0^L pB\,\frac{\delta w}{\delta q_i}\mathrm{d}x\,\delta q_i = \sum_i Q_{\mathrm{ext},i}\delta q_i \ . \tag{22}$$

The virtual work due to plastic dissipation at the two hinges can be expressed as

$$\begin{aligned}\delta W_{\mathrm{diss}} &= \sum_i Q_{\mathrm{diss},i}\delta q_i \\ &= M_{\mathrm{sup}}\delta\theta_{\mathrm{pl,sup}} - N\,\delta\Delta l_{\mathrm{pl,sup}} - Q_{\mathrm{pl,sup}}\delta w_{\mathrm{pl,sup}} - M_{\mathrm{mid}}\delta\theta_{\mathrm{pl,mid}} - N\,\delta\Delta l_{\mathrm{pl,mid}} = \\ &= M_{\mathrm{sup}}\delta\theta_{\mathrm{pl,sup}} - N\,\delta\Delta l_{\mathrm{pl,sup}} - Q_{\mathrm{pl,sup}}\delta w_{\mathrm{pl,sup}} - M_{\mathrm{mid}}\sum_i \frac{\partial\theta_{\mathrm{pl,mid}}}{\partial q_i}\delta q_i - N\,\delta\Delta l_{\mathrm{pl,mid}},\end{aligned} \tag{23}$$

providing the definitions of the dissipative forces $Q_{\mathrm{diss},i}$ used in eq. (17). An example of the equations of motion obtained from (17) is given in Appendix A for the case of a purely elastic response.

2.2.2 Response after wave motion

We proceed to analyse the response in Phases IIa, IIIa, IV and V, which do not feature propagation of elastic flexural waves or travelling plastic hinges (see Fig. 4). Fourth-order polynomial shape functions are again assumed and the following boundary conditions are imposed

$$\begin{aligned} &w(x=0) = w_{\mathrm{pl,sup}}, \qquad \frac{\partial w}{\partial x}(x=0) = \theta_{\mathrm{pl,sup}}, \qquad w(x=L) = w_0, \\ &\frac{\partial w}{\partial x}(x=L) = \theta_{\mathrm{pl,mid}}, \qquad \frac{\partial^3 w}{\partial x^3}(x=L) = 0 \end{aligned} \tag{24}$$

giving

$$\begin{aligned} w(x,t) = {} & w_{\mathrm{pl,sup}}(t) + x\theta_{\mathrm{pl,sup}}(t) - \frac{x^2}{2L^2}\left(8w_{\mathrm{pl,sup}}(t) - 8w_0(t) + 3L\theta_{\mathrm{pl,mid}}(t) + 5L\theta_{\mathrm{pl,sup}}(t)\right) \\ & + \left(\frac{2x^3}{L^3} - \frac{x^4}{2L^4}\right)\left(2w_{\mathrm{pl,sup}}(t) - 2w_0(t) + L\theta_{\mathrm{pl,mid}}(t) + L\theta_{\mathrm{pl,sup}}(t)\right). \end{aligned} \tag{25}$$

The generalised coordinates in these phases of the response are taken as

$$\mathbf{q} = \left[w_0, \theta_{\mathrm{pl,sup}}, w_{\mathrm{pl,sup}}, \Delta l_{\mathrm{pl,sup}}, \theta_{\mathrm{pl,mid}}, \Delta l_{\mathrm{pl,mid}} \right]^{\mathrm{T}}. \tag{26}$$

Equations of motions are obtained from eq. (17).

2.3 Numerical integration of the equations of motion

Equations (17) represent a system of differential-algebraic equations of differential index three [22],[23] . An index reduction method proposed by Gear [24] is used. This formulation reduces the differential index to two. A general second order index three system arising from constrained mechanical systems has the form [22]

$$\begin{aligned} \dot{\mathbf{q}} &= \mathbf{v}, \\ \mathbf{M}(\mathbf{q})\dot{\mathbf{v}} &= \mathbf{f}(\mathbf{q},\mathbf{v}) - \mathbf{G}^{\mathrm{T}}(\mathbf{q})\boldsymbol{\lambda}, \\ \mathbf{0} &= \mathbf{g}(\mathbf{q}), \end{aligned} \tag{27}$$

involving the generalised coordinates $\mathbf{q}$, the generalised velocities $\mathbf{v}$, the Lagrange multipliers $\boldsymbol{\lambda}$, the generalised mass matrix $\mathbf{M}$, the holonomic constraints $\mathbf{g}(\mathbf{q})$ and $\mathbf{G} = \partial \mathbf{g} / \partial \mathbf{q}$. The non-holonomic constraints are not included here, because no action is required on them during index reduction.

Gear [24] proposed to reformulate the system as

$$\begin{aligned} \dot{\mathbf{q}} &= \mathbf{v} - \mathbf{G}^{\mathrm{T}}(\mathbf{q})\boldsymbol{\mu}, \\ \mathbf{M}(\mathbf{q})\dot{\mathbf{v}} &= \mathbf{f}(\mathbf{q},\mathbf{v}) - \mathbf{G}^{\mathrm{T}}(\mathbf{q})\boldsymbol{\lambda}, \\ \mathbf{0} &= \mathbf{g}(\mathbf{q}), \\ \mathbf{0} &= \mathbf{G}\mathbf{v}, \end{aligned} \tag{28}$$

introducing additional Lagrange multipliers $\boldsymbol{\mu}$. This system (28) is of differential index two and can be integrated using the variable-order, variable-step backward difference method implemented in the *Sundials-IDA* solver [25] included in the *Python* package *Assimulo* [26].

Across transitions from one phase of the response to the next it is imposed that the total energy in the system is conserved; consistent systems of initial conditions are imposed ensure that constraints are satisfied across the transition.

3 FINITE ELEMENT MODELLING

Two-dimensional Finite Element (FE) simulations of the transverse pressure loading of the beams were conducted in ABAQUS Explicit [27] to compare with the analytical predictions. Following a preliminary mesh convergence study, half of the beam was discretised with 1000 beam elements of type B21, which model the effects of elastic deflections due to shear and rotary inertia. An encastre boundary condition was defined at the support and symmetry in direction x was enforced at mid-span. The load was applied as a transverse, time dependent pressure.

The response of the material was taken as isotropic linear elastic ($E = 200\text{GPa}$, $\nu = 0.3$) followed by incompressible *J2* plasticity ($\sigma_y = 300\text{MPa}$) with negligible strain hardening. The bulk viscosity were left at their default values. The density was taken as $\rho = 7850\ \text{kgm}^{-3}$, representative of steel. We note that the analyses cannot capture plastic shear deformations of the beam, while are modelled in the analytical calculation. The cross-section Poisson's ratio was set to 0 for all computations in this study; this excludes the effect of necking due to large plastic strains, which is not modelled analytically.

The FE predictions are processed to record the mid-span deflection w_0 and the wave front position $x = \xi$; this is taken, at every time, as the location where the bending moment attains a local maximum (the maximum closest to the support is considered). For the hinge located at the support we compare FE predictions of the plastic stretching and plastic rotation to the corresponding analytical predictions $\Delta l_{\text{pl,sup}}, \theta_{\text{pl,sup}}$. To this effect we consider a portion of the length of the beam, l_{zone}, adjacent to the support; for this portion, the normal plastic strains at the top and bottom surface of the beam are extracted ($\varepsilon_{\text{pl,11,top},i}$ and $\varepsilon_{\text{pl,11,bottom},i}$, respectively), and estimates of the plastic stretching and plastic rotation are obtained as

$$\Delta l_{\text{pl,sup,FE}} = \frac{l_{\text{zone}}}{n_{\text{e}}} \sum_{i=1}^{n_{\text{e}}} \frac{1}{2} (\varepsilon_{11,\text{pl,top},i} + \varepsilon_{11,\text{pl,bottom},i}) \ , \tag{29}$$

$$\theta_{\text{pl,sup,FE}} = \frac{l_{\text{zone}}}{n_{\text{e}}} \sum_{i=1}^{n_{\text{e}}} \frac{1}{2} (\varepsilon_{11,\text{pl,top},i} - \varepsilon_{11,\text{pl,bottom},i}) , \tag{30}$$

where n_{e} denotes the number of elements within the length l_{zone}. The total plastic elongation of the beam was computed from eq. (29) with the choice $l_{\text{zone}} = L$.

4 RESULTS AND DISCUSSION

In this Section we compare theoretical and analytical predictions of the response of a clamped beam to transverse pressure loading, to assess the accuracy of the theoretical predictions. Then, the theoretical models are used to construct non-dimensional regime maps to aid design of beams subject to dynamic loading.

4.1 Pressure history and dimensional analysis

The proposed model can predict the response of a clamped beam subject to an arbitrary pressure history uniformly distributed on the beam's surface. To limit the parameter space, the loading is idealised as a pressure history of triangular shape and total time duration t_{i}, comprising a linear rise phase to a pressure $p_{\max}$ in a time $\alpha_{\mathrm{r}} t_{\mathrm{i}}$, followed by a linear fall phase to negligible pressure in a time $(1-\alpha_{\mathrm{r}})t_{\mathrm{i}}$, where $\alpha_{\mathrm{r}} \in [0,1]$. Mathematically

$$p(t) = \begin{cases} \dfrac{p_{\max}}{\alpha_{\mathrm{r}} t_{\mathrm{i}}} t, & 0 \le t \le \alpha_{\mathrm{r}} t_{\mathrm{i}}, \\ \dfrac{p_{\max}}{t_{\mathrm{i}}(1-\alpha_{\mathrm{r}})}(t_{\mathrm{i}} - t), & \alpha_{\mathrm{r}} t_{\mathrm{i}} < t \le t_{\mathrm{i}}, \\ 0, & t > t_{\mathrm{i}}. \end{cases} \tag{31}$$

The overall impulse per unit area follows as

$$I_{\mathrm{p}} = \int_0^t p(t)\mathrm{d}t = \frac{1}{2} p_{\max} t_{\mathrm{i}}. \tag{32}$$

Dimensional analysis dictates that the problem under investigation depends on the following set of non-dimensional groups. The solution sought is represented by the set

$$\begin{aligned} &\bar{w}_0 = \frac{w_0}{L}, && \bar{\xi} = \frac{\xi}{L}, && \theta_{\mathrm{pl,sup}}, \\ &\bar{w}_{\mathrm{pl,sup}} = \frac{w_{\mathrm{pl,sup}}}{L}, && \overline{\Delta l}_{\mathrm{pl,sup}} = \frac{\Delta l_{\mathrm{pl,sup}}}{L}, && \theta_{\mathrm{pl,mid}}, \\ &\overline{\Delta l}_{\mathrm{pl,mid}} = \frac{\Delta l_{\mathrm{pl,mid}}}{L} && \tau = \frac{t}{L\sqrt{\frac{\rho}{\sigma_{\mathrm{y}}}}}; \end{aligned} \tag{33}$$

The geometry of the beam and constitutive response of the material are represented by the parameters

$$\bar{H} = \frac{H}{L}, \qquad \bar{E} = \frac{E}{\sigma_y}. \tag{34}$$

The loading is described by

$$\bar{p}_{max} = \frac{\bar{p}_{max}}{\sigma_y}, \qquad \tau_i = \frac{t_i}{L\sqrt{\frac{\rho}{\sigma_y}}}, \qquad \alpha_r, \qquad \bar{I}_p = \frac{I_p}{L\sqrt{\rho\sigma_y}} = \frac{1}{2}\bar{p}_{max}\tau_i \ . \tag{35}$$

4.2 Model Validation

In this section we explore the accuracy of the analytical predictions over wide ranges of the non-dimensional parameters $\bar{I}_p$, τ_i, α_r, $\bar{H}$. In all FE simulations the half beam length was arbitrarily set to $L = 1\,\mathrm{m}$; the material properties were such to have $\bar{E} = E/\sigma_y \approx 666$, representative of the case of mild steel. The imposed initial conditions are

$$\bar{w}_0(\tau = 0) = 10^{-8}, \qquad \bar{w}_0'(\tau = 0) = 0, \qquad \bar{\xi}(\tau = 0) = 10^{-2}, \qquad \bar{\xi}'(\tau = 0) = 0. \tag{36}$$

Note that the non-zero initial conditions for $\bar{w}_0$ and $\bar{\xi}$ are due to avoid divisions by zero in the integration of the equations of motion (see Appendix A).

In Figs. 5-7 we present analytical and FE predictions of the peak beam deflection $\bar{w}_{0,max}$ and the corresponding non-dimensional time at which this peak deflection is attained, τ_{max}. The results are shown for three different aspect ratios, two different applied impulses and two different values of α_r. Excellent agreement between theoretical and FE predictions is found. We note that low values of τ_i correspond to high pressures applied for short amount of time (‘impulsive’ loading); in contrast, large values of τ_i indicate long time durations with low applied pressure (‘quasi-static’ loading).

For all aspect ratios the beams it is clear that in the impulsive regime the response is scarcely dependent upon τ_i and α_r. If the load duration t_i is comparable or larger than the characteristic response time $L\sqrt{\rho/\sigma_y}$, i.e. τ_i is sufficiently large, the response is sensitive to the non-dimensional load duration τ_i. The predictions are scarcely sensitive to α_r, defining the shape of the pressure history, in the impulsive regime; in contrast, for large values of τ_i, the response is affected by the value of α_r. The model effectively captures the transition from

impulsive to quasi-static loading. We note that in the impulsive regime the non-dimensional time at peak deflection $\tau_{\max}$ is close to 1, indicating that the response time of the structure approaches the characteristic response time $L\sqrt{\rho/\sigma_y}$, which is proportional to the period of oscillation of an elastic string under tensile stress σ_y, as remarked by Fleck [7].

4.3 Detailed comparison of analytical and FE predictions

We proceed to a detailed comparison of analytical and FE predictions. This is done for two cases: the first corresponds to a relatively slow loading, representative of deflagration incidents [13, 14]

$$\bar{H} = 0.00286, \qquad \tau_i = 20, \qquad \bar{p}_{\max} = 3\ 10^{-4}, \qquad \alpha_r = 0.5. \tag{37}$$

The second case corresponds to impulsive loading, with high pressure applied for short time duration; the relevant non-dimensional groups are

$$\bar{H} = 0.00444, \qquad \tau_i = 0.01, \qquad \bar{p}_{\max} = 0.06, \qquad \alpha_r = 0.5. \tag{38}$$

The histories of mid-span deflection $\bar{w}_0$ and wave front position $\bar{\xi}$ are analysed in Fig. 8 for case 1. The response of the beam is elastic-plastic; the structure reaches a peak deflection before undergoing a retardation phase. Elastic vibrations are evident in Fig. 8a; the vertical dashed lines in this figure denote phase transitions, as indicated. Figure 8b shows an elastic flexural wave rapidly propagating towards mid-span, reaching this point at $\tau \approx 3.41$, corresponding to transition into Phase IIa. Shortly after, plasticity is attained at the support, corresponding to the onset of Phase IIIa. With continued loading, the beam then switches to Phase IV (corresponding to yielding at mid-span) and finally undergoes an elastic relaxation phase (Phase V). It is observed that the beam can switch between Phases IV and V if the applied pressure keeps increasing, as a consequence of the elastic vibrations. We note that the predictions of the analytical model are in excellent agreement with those of detailed FE simulations.

Next we consider, in Fig. 9a, the predictions of kinetic energy, elastic strain energy and plastic work; these energies are presented in non-dimensional form $\bar{E}$, normalised by the characteristic energy $V_{\max}$ (eq. (11)). First, we note that FE and analytical predictions are in good agreement. The response is initially dominated by elasticity (Phase I, IIa) but then

plastic dissipation is triggered upon transition into Phase IIIa; such plastic dissipation if comparable to the elastic strain energy, such that both elastic and plastic deformation need to be modelled.

In Fig. 9b we present predicted histories of the generalised stresses N, M, Q, normalised by their corresponding maximum values N_0, M_0, Q_0, respectively. The two sets of predictions are in broad agreement. For this slender beam shear forces are small compared to axial forces and bending moments; the response is bending-dominated in the initial phases (I, IIa), but they become stretching-dominated in the latest phases (IIIa, IV, V).

Figure 10 presents time histories of the plastic rotation at the support as well as plastic stretching. The FE predictions suggest that plasticity occurs earlier than predicted by the analytical model; on the other hand, the analytical model assumes that entire cross-sections of the beam undergo plastic deformation, while the FE simulations account for progressive yielding of the cross-section. The FE and analytical predictions of plastic rotation at the support and total plastic stretching are in good agreement; both sets suggest that first the beam undergoes substantial plastic rotation at the support, followed by plastic stretching.

We proceed by presenting the results for mid-span deflection and wave front position for case 2 (Fig. 11). Good agreement is observed between analytical model and FE predictions. The transitions between the response phases are indicated in the figure: yield at the support occurs almost instantaneously (onset of Phase IIb), and a travelling plastic hinge develops later in time (Phase IIIb). The mid-span deflection increases until the travelling plastic hinge reaches the mid-span and a plastic retardation phase occurs (Phase IV).

In Fig. 12a, the normalised energy components are presented for case 2. Excellent agreement is observed between FE and analytical predictions. In this case, in the initial phase of the response high kinetic energy is imparted to the beam and partly converted into elastic strain energy and plastic dissipation; this dissipation is substantially larger than the elastic strain energy. The evolution of the normalised generalised stresses at the support is presented in Fig. 12b, which shows excellent agreement between FE and theoretical predictions. The very early stages of the response are characterised by high values of shear forces and bending

moment at the support; with continued deflection, the bending moment decreases while the stretching forces increase.

In Fig. 13 we present the time history of plastic rotation at the support and stretching. Good agreement between the analytical and numerical predictions is evident. The plastic rotation increases earlier than the plastic stretching, in line with the data in Fig. 12b.

4.4 Regime Maps

The validated analytical model is now used to construct design maps for a clamped beam subject to arbitrary transverse pressure histories. Four different regimes of response were identified in this study, namely:

- Regime A: elastic response;
- Regime B: elastic response followed by plastic hinge formation at the support;
- Regime C: elastic response followed by formation of stationary plastic hinges at the support and mid-span;
- Regime D: elastic response followed by formation of a stationary plastic hinge at the support and a travelling plastic hinge along the beam span.

The regime maps were constructed to be representative of steel structures, with $\bar{E} = 666.$ In all cases the rise time of the triangular pressure history was taken as 50% of the total loading time, i.e. $\alpha_r = 0.5$. The response of the beam is therefore only affected by the non-dimensional groups $\bar{H}$, $\bar{I}_p$ and τ_i; three maps were produced to illustrate the sensitivity of the response to these three governing parameters.

Figure 14 presents a map for the choice $\bar{I}_p = 3\,10^{-4}$, illustrating the different regimes of response. The dotted lines represent contours of the peak mid-span deflection. Slender beams and the short loading time promote a response dominated by plasticity and large deflection. The dashed lines indicate simple analytical estimates for the onset of plastic deformation in the beam response. The cross denotes the 'case 2' problem analysed in detail in Section 4.3.

The curve labelled $\bar{p}_{max} = \bar{p}_c$ corresponds to the quasi-static plastic collapse load of a rigid-perfectly plastic fully clamped beam, given by Jones [2]

$$\bar{p}_c = \frac{p_c}{\sigma_y} = \frac{4M_0}{BL^2\sigma_y} = \bar{H}^2 . \tag{39}$$

For load times $\tau_i > 1$, eq. (39) is in broad agreement with the transition between regimes A and B predicted by the analytical model (recall that regime A indicates elastic response, while regime B includes yield at the support). For short loading time, $\tau_i < 1$, the response of the beam is impulsive; an estimate of the minimum impulse to cause plastic collapse of a cross-section is obtained as follows. The initial velocity of the beam can be written

$$v_0 = \frac{I_p}{\rho H} , \tag{40}$$

Resulting in a kinetic energy

$$T_0 = \frac{1}{2}\rho BHLv_0^2 = \frac{BLI_p^2}{2\rho H} . \tag{41}$$

We assume this kinetic energy is converted to elastic bending strain energy; using the deflection profile (25) and ($|M|(x=0) = M_0$), the strain energy reads

$$V_{bend,max} = \frac{3B\sigma_y^2 LH}{40E} . \tag{42}$$

Equating (41) to (42) and solving for I_p yields

$$I_{p,min} = \sqrt{\frac{3\sigma_y^2 \rho H^2}{20E}} \tag{43}$$

or in non-dimensional form

$$\bar{I}_{p,min} = \sqrt{\frac{3}{20}}\frac{\bar{H}}{\sqrt{\bar{E}}} \approx 0.387\frac{\bar{H}}{\sqrt{\bar{E}}} . \tag{44}$$

It is clear from Fig. 14 that eq. (44) provides a conservative prediction of the minimum impulse to attain a fully plastic cross-section. Equations (39) and (44) can be used as quick conservative design formulae to guarantee that the beam response is predominantly elastic; the map in Fig. 14 allows less conservative and more accurate designs.

In Fig. 15 we examine the effects of load duration and non-dimensional impulse, for the choice $\bar{H} = 0.01$. The limit cases (39) and (44) are included in the map and again provide a conservative estimate of the boundary between regimes A and B. As expected, high applied

impulse and short loading time promote inelastic response and the dynamic travelling plastic hinge mechanism.

Finally, in Fig. 16, we consider a constant load duration $\tau_i = 20$ and we explore the effects of geometry and applied impulse. The cross denotes the 'case 1' problem analysed in detail in Section 4.3. Since the chosen loading time $\tau_i = 20$ is relatively high, the impulsive limit (44) is not applicable, while the quasi-static limit (39) is very conservative in this case. On the other hand the analytical model predicts accurately the transitions between regimes of behaviour and serves an effective design tool.

The detailed predictions of the proposed analytical model allow estimating strain distributions in the beam and can be used, in conjunction with a material-specific failure criterion, to predict failure of the structure by different mechanisms, including shear-off and tensile tearing. A modified version of the proposed calculation could handle the case of a beam with elastic axial, transverse or rotational supports. The model should be modified to include in the Lagrangian the elastic energy stored in the supporting springs, and boundary conditions (eq. (5)) should be adapted to include the additional degrees of freedom. The model would then be able to predict the effect of support compliance upon the response of the beam, including the emergence and evolution of plastic hinges and plastic stretching. This is left as a topic for future studies. These are left as topics for future studies.

5 CONCLUSIONS

An analytical model was formulated to predict the dynamic response of clamped beams made from an elastic-plastic material to arbitrary pressure loading histories. The model was validated by detailed Finite Element simulations over wide ranges of loading and geometric parameters. The non-dimensional governing parameters of the problem and distinct regimes of response were identified and the model was used to construct effective design maps.

The main conclusions from the study are as follows:

- Assuming an elastic-plastic material response allows effective predictions of the dynamic response of a clamped beam to arbitrary loading; it allows capturing the

transitions between response regimes and an accurate estimate of the stress fields at any time.

- The initial dynamic response of clamped beams is governed by propagation of elastic flexural waves and beam stretching; such elastic response may be followed, for ductile materials, by an elastic-plastic phase in which plasticity occurs, typically at the supports. In case of intense loading, slender beams and short time duration, a travelling plastic hinge phase can also be induced.
- Design maps are provided to allow effective sizing of beams subject to transverse pressure loading ranging from quasi-static to impulsive.

ACKNOWLEDGEMENTS

The research was funded, motivated and steered by the Turbomachinery Engineering team (Drs S. Rossin, V. Bisio, D. Zaffino) of GE Oil & Gas.

Appendix A. Equations of motion for Phases I and IIa

a) Phase I

First equation of motion

$$\rho BH\left(\left(\left(\frac{32H^2}{315\xi}-\frac{187\xi}{315}+L\right)\ddot{w}_0-\left(\frac{187\,w_0}{630}+\frac{16H^2 w_0}{315\xi^2}\right)\ddot{\xi}-\left(\frac{187}{315}+\frac{32H^2}{315\xi^2}\right)\dot{w}_0\dot{\xi}-\left(\frac{4H^2}{21\xi^3}+\frac{92}{315\xi}\right)w_0\dot{\xi}^2\right)\right. \quad (45)$$
$$\left.+EBH\left(\frac{16H^2 w_0}{15\xi^3}+\frac{8192\,w_0^3}{11025L\xi^2}\right)=Bp\left(L-\frac{7\xi}{15}\right)\right.$$

Second equation of motion

$$\rho BH\left(\begin{array}{l}\left(\left(-\frac{187\,w_0}{630}-\frac{16H^2 w_0}{315\xi^2}\right)\ddot{w}_0+\left(\frac{92H^2 w_0^2}{315\xi^3}+\frac{92w_0^2}{315\xi}\right)\ddot{\xi}\right.\\ \left.+\left(\frac{184\,w_0}{315\xi}+\frac{184H^2 w_0}{315\xi^3}\right)\dot{w}_0\dot{\xi}-\left(\frac{46}{315\xi^2}+\frac{46H^2}{105\xi^4}\right)w_0^2\dot{\xi}^2\right)\end{array}\right. \quad (46)$$
$$\left.-EBH\left(\frac{8H^2 w_0^2}{5\xi^4}+\frac{4096w_0^4}{11025L\xi^3}\right)=-\frac{7Bp\,w_0}{15}\right.$$

b) Phase IIa

Equation of motion

$$\rho BH\,\frac{32\left(H^2+4L^2\right)}{315L}\ddot{w}_0+EBH\left(\frac{16H^2}{15L^3}w_0+\frac{8192}{11025L^3}w_0^3\right)=\frac{8BLp}{15}\ . \quad (47)$$

References

[1] T.X. Yu, Elastic Effects in the Dynamic Plastic Response of Structures, in: N.W. Jones, T. (Ed.) Structural Crashworthiness and Failure, Elsevier, University of Liverpool, 1993, pp. 341-384.
[2] N. Jones, Structural impact, Cambridge, 1989.
[3] S.B. Menkes, H.J. Opat, Broken beams, Experimental Mechanics, 13 (1973) 480-486.
[4] P.S. Symonds, Large Plastic Deformations of Beams Under Blast
Type Loading, in: Proceedings of the Second U.S. National Congress of Applied Mechanics, 1954, pp. 505–515.
[5] N. Jones, A theoretical study of the dynamic plastic behavior of beams and plates with finite-deflections, International Journal of Solids and Structures, 7 (1971) 1007-1029.
[6] N. Jones, Plastic failure of ductile beams loaded dynamically, J Eng Ind Trans ASME, 98 Ser B (1976) 131-136.
[7] N.A. Fleck, V.S. Deshpande, The Resistance of Clamped Sandwich Beams to Shock Loading, Journal of Applied Mechanics, 71 (2004) 386.
[8] W.Q. Shen, N. Jones, A failure criterion for beams under impulsive loading, International journal of impact engineering, 12 (1992) 101-121.
[9] T.X. Yu, F.L. Chen, A further study of plastic shear failure of impulsively loaded clamped beams, International Journal of Impact Engineering, 24 (2000) 613-629.
[10] H.M. Wen, Deformation and tearing of clamped work-hardening beams subjected to impulsive loading, International Journal of Impact Engineering, 18 (1996) 425-433.
[11] E.H. Lee, P.S. Symonds, Large plastic deformations of beams under transverse impact, American Society of Mechanical Engineers -- Transactions -- Journal of Applied Mechanics, 19 (1952) 308-314.
[12] P.S. Symonds, C.W.G. Frye, On the relation between rigid- plastic and elastic- plastic predictions of response to pulse loading, International Journal of Impact Engineering, 7 (1988) 139-149.
[13] American Petroleum Institute, API RP 2FB - Recommended Practice for the Design of Offshore Facilities Against Fire and Blast Loading, in, 2006.
[14] Det Norske Veritas, DNV-RP-C204: Design against accidental loads, in, 2010.
[15] G.K. Schleyer, S.S. Hsu, A modelling scheme for predicting the response of elastic–plastic structures to pulse pressure loading, International Journal of Impact Engineering, 24 (2000) 759-777.
[16] Y. Yuan, P.J. Tan, K.A. Shojaei, P. Wrobel, Large deformation, damage evolution and failure of ductile structures to pulse-pressure loading, International Journal of Solids and Structures, 96 (2016) 320-339.
[17] K.F. Graff, Wave motion in elastic solids, Oxford : Clarendon Press, Oxford, 1975.
[18] T.X. Yu, J.L. Yang, S.R. Reid, Interaction between reflected elastic flexural waves and a plastic `hinge' in the dynamic response of pulse loaded beams, International Journal of Impact Engineering, 19 (1997) 457-475.
[19] A. Schiffer, V.L. Tagarielli, The dynamic response of composite plates to underwater blast: Theoretical and numerical modelling, International Journal of Impact Engineering, 70 (2014) 1-13.
[20] C. Lanczos, The variational principles of mechanics, 4th ed. ed., New York : Dover Publications, New York, 1986.
[21] P. Hamill, A student's guide to Lagrangians and Hamiltonians, Cambridge : Cambridge University Press, 2014.

[22] U.M. Ascher, Computer methods for ordinary differential equations and differential-algebraic equations, Philadelphia : Society for Industrial and Applied Mathematics, Philadelphia, 1998.
[23] O.A. Bauchau, Flexible multibody dynamics, Dordrecht : Springer, Dordrecht, 2011.
[24] C.W. Gear, B. Leimkuhler, G.K. Gupta, Automatic integration of Euler-Lagrange equations with constraints, Journal of Computational and Applied Mathematics, 12 (1985) 77-90.
[25] A.C. Hindmarsh, P.N. Brown, K.E. Grant, S.L. Lee, R. Serban, D.E. Shumaker, C.S. Woodward, SUNDIALS: Suite of nonlinear and differential/algebraic equation solvers, ACM transactions on mathematical software, 31 (2005) 363-396.
[26] C. Andersson, C. Führer, J. Åkesson, Assimulo: A unified framework for ODE solvers, Mathematics and Computers in Simulation, 116 (2015) 26-43.
[27] Abaqus, Analysis User's Manual 6.14, Dassault Systèmes Simulia Corp., 2014.

Figures

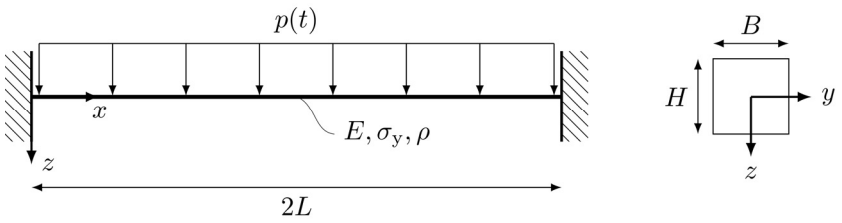

Figure 1. Fully clamped beam subject to uniform pressure loading.

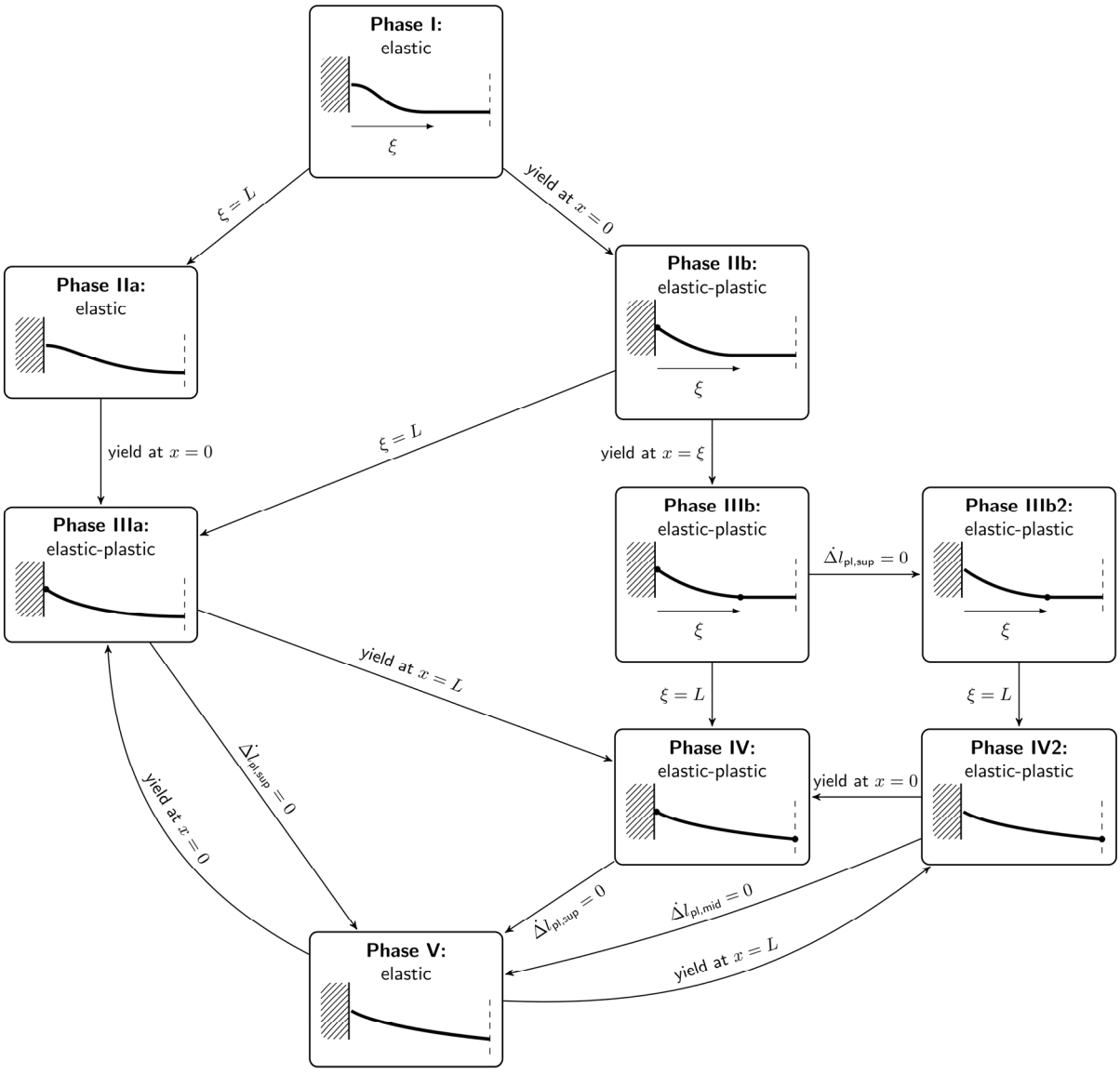

Figure 2. Schematics of the possible phases of beam response.

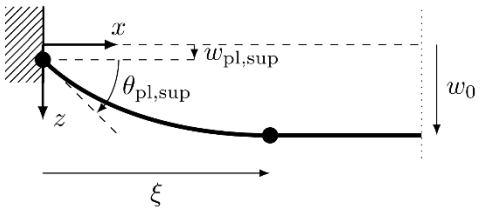

Figure 3. Deformation profile and degrees of freedom for wave propagation modes.

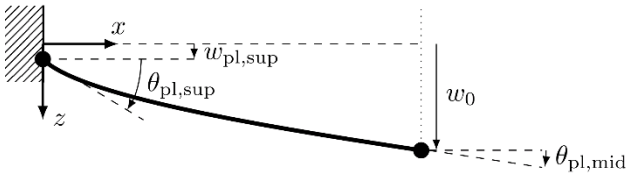

Figure 4. Deformation profile and degrees of freedom for stationary modes.

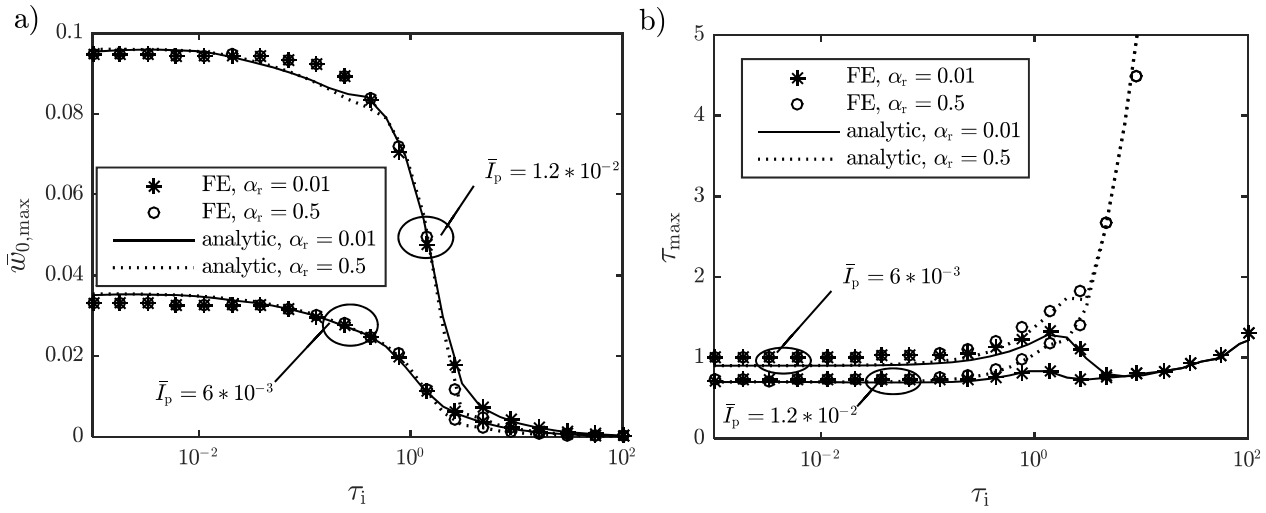

Figure 5. Comparison of maximum mid-span deflection (a) and time at maximum deflection (b) obtained from FE and the analytical model for $\bar{H} = 0.1$, two different impulses and two different loading shape parameters.

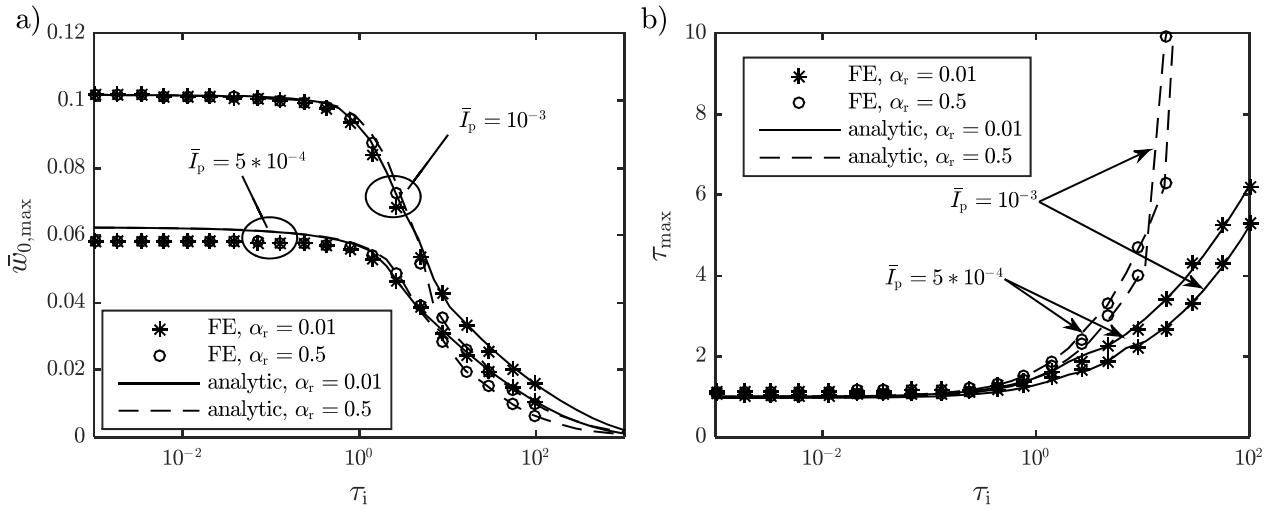

Figure 6. Comparison of maximum mid-span deflection (a) and time at maximum deflection (b) obtained from FE and the analytical model for $\bar{H} = 0.01$, two different impulses and two different loading shape parameters.

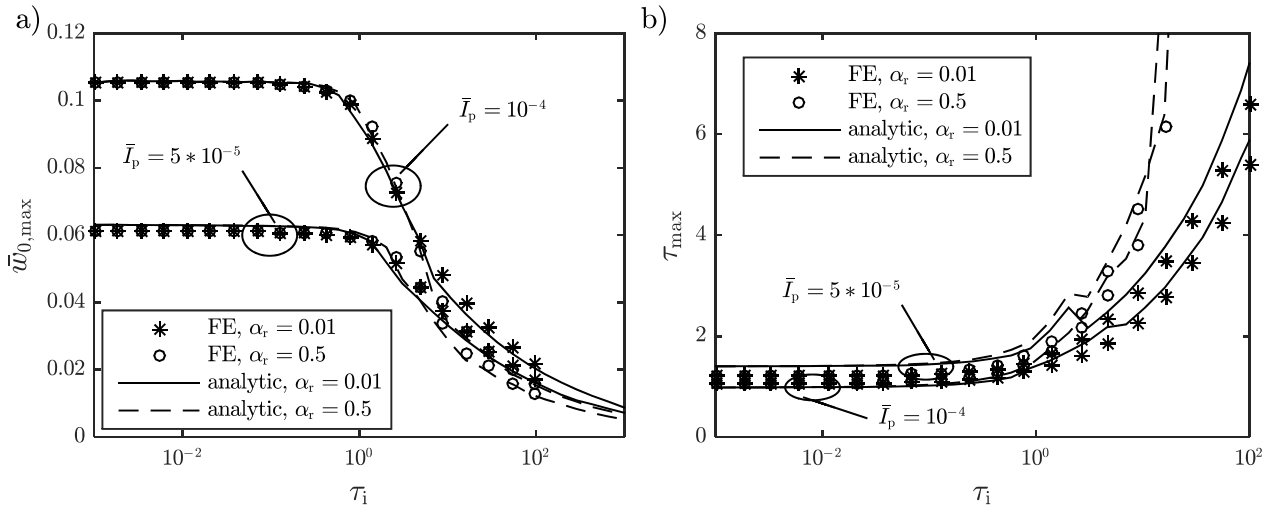

Figure 7. Comparison of maximum mid-span deflection (a) and time at maximum deflection (b) obtained from FE and the analytical model for $\bar{H} = 0.001$, two different impulses and two different loading shape parameters.

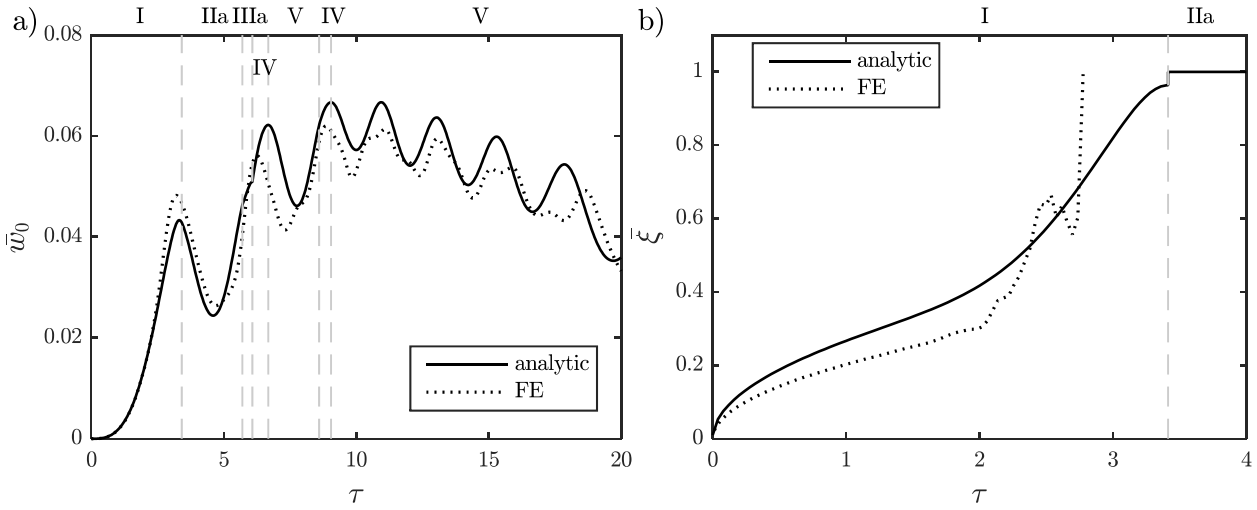

Figure 6. Comparison of mid-span deflection (a) and wave front position (b) obtained from FE analysis and the analytical model for case 1.

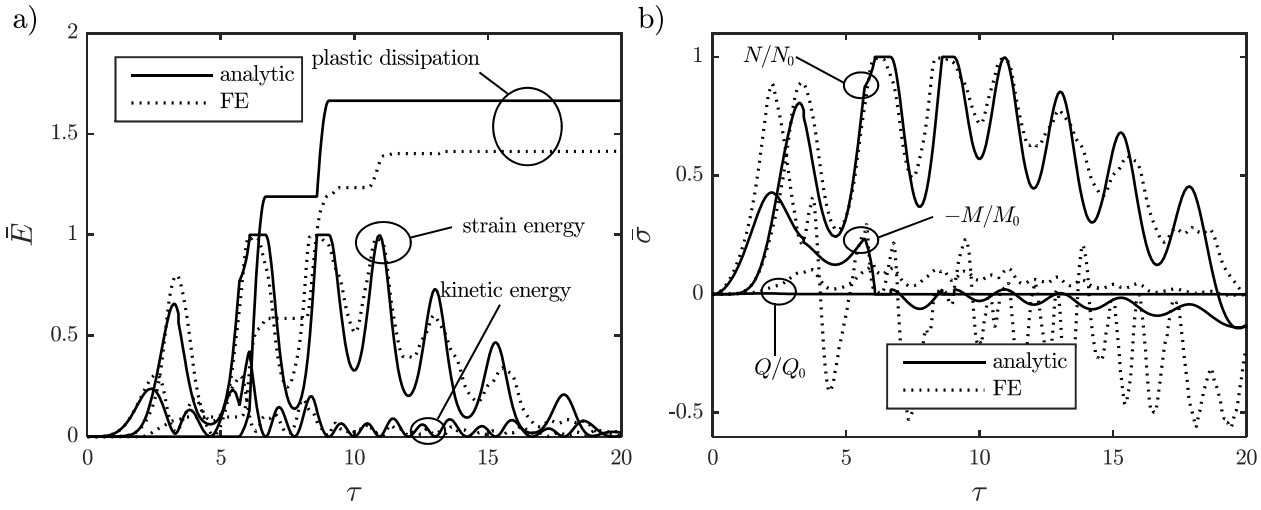

Figure 7. Comparison of kinetic and potential energy and plastic dissipation (a) and generalised stresses at the support (b) obtained from FE analysis and the analytical model for case 1.

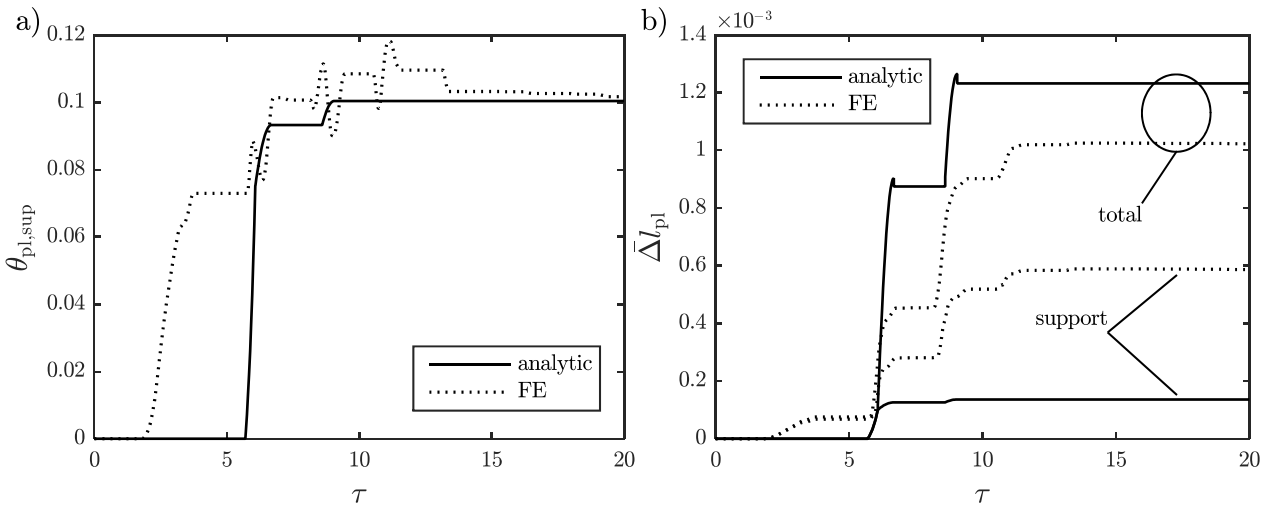

Figure 8. Comparison of plastic angle (a) and plastic elongation (b) at the support obtained from FE analysis and the analytical model for case 1.

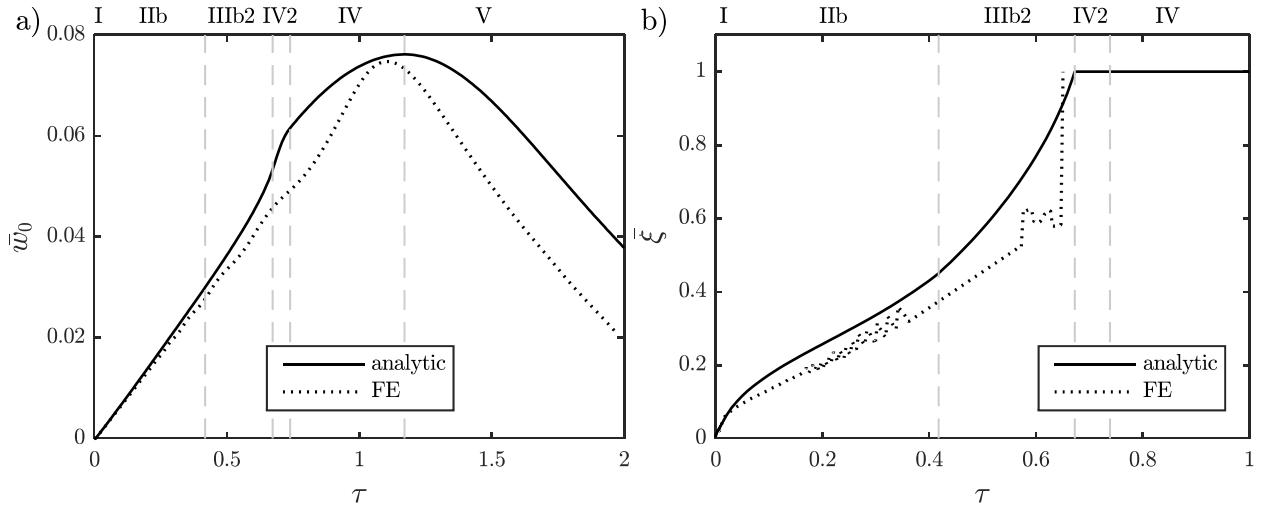

Figure 9. Comparison of mid-span deflection (a) and wave front position (b) obtained from FE analysis and the analytical model for case 2.

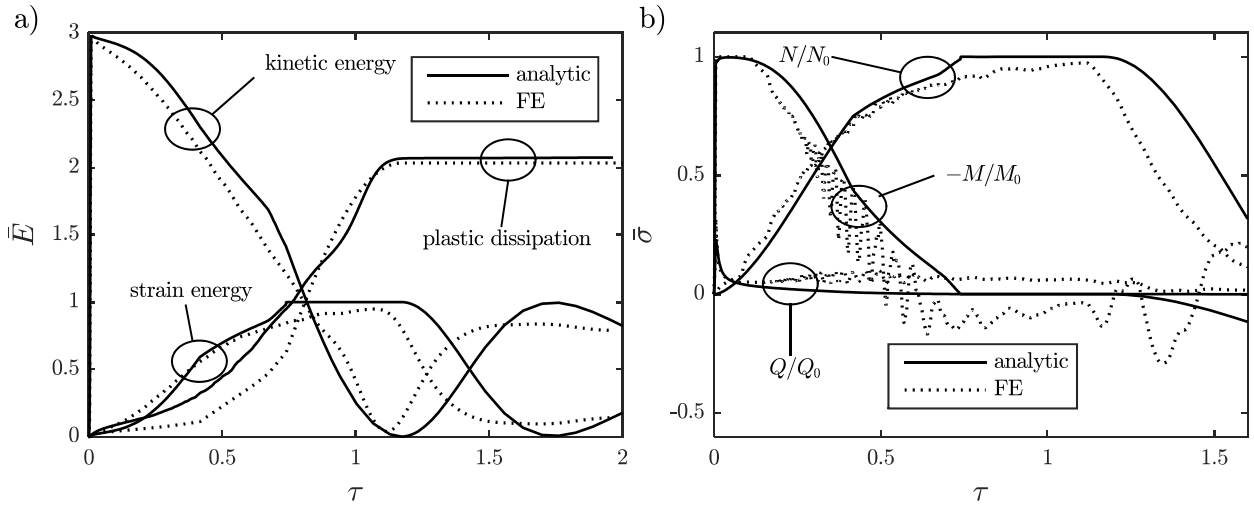

Figure 10. Comparison of kinetic and potential energy and plastic dissipation (a) and generalised stresses at the support (b) obtained from FE analysis and the analytical model for case 2.

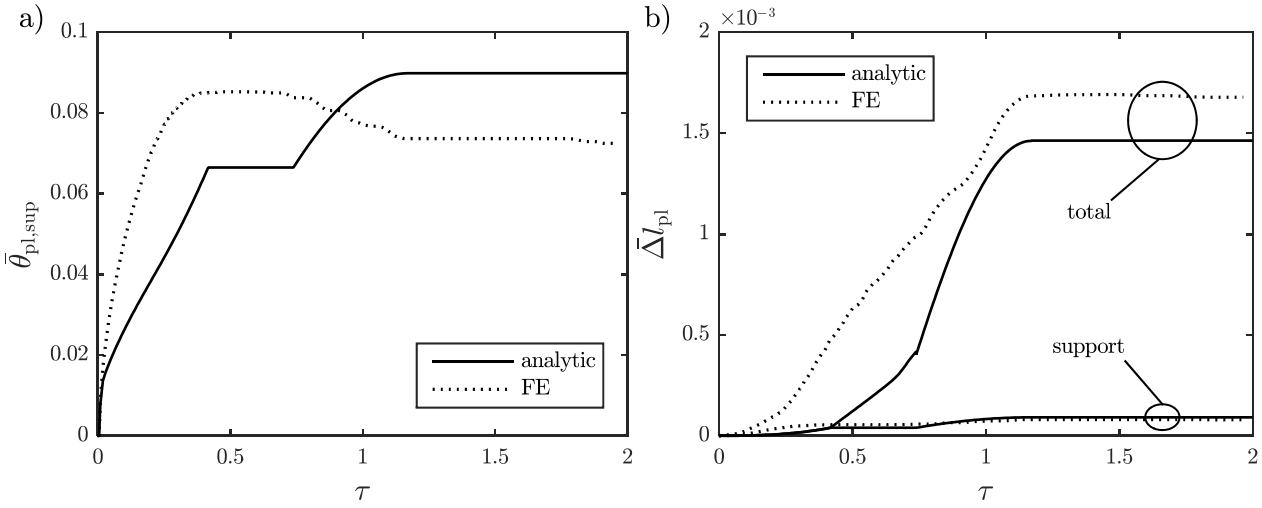

Figure 11. Comparison of plastic angle (a) and plastic elongation (b) at the support obtained from FE analysis and the analytical model for case 2.

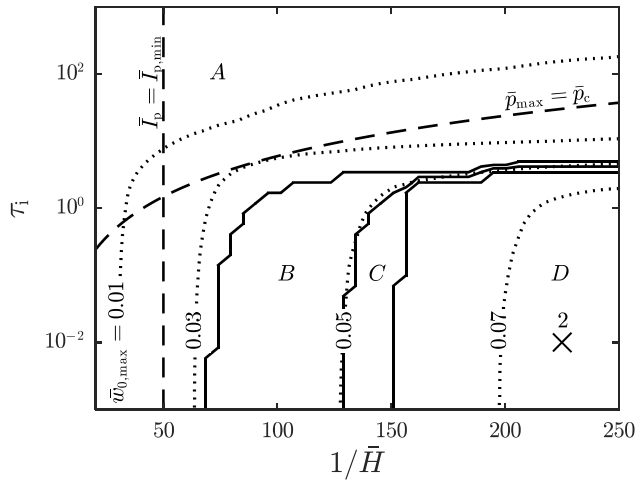

Figure 12. Regimes of behaviour and contours of maximum mid-span deflection for $\bar{I}_p = 3\ 10^{-4}, \alpha_r = 0.5$.

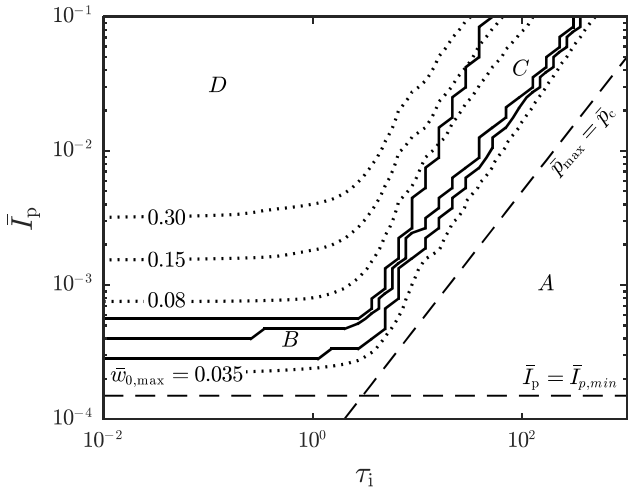

Figure 13. Regimes of behaviour and contours of maximum mid-span deflection for $\bar{H} = 0.01, \alpha_r = 0.5$.

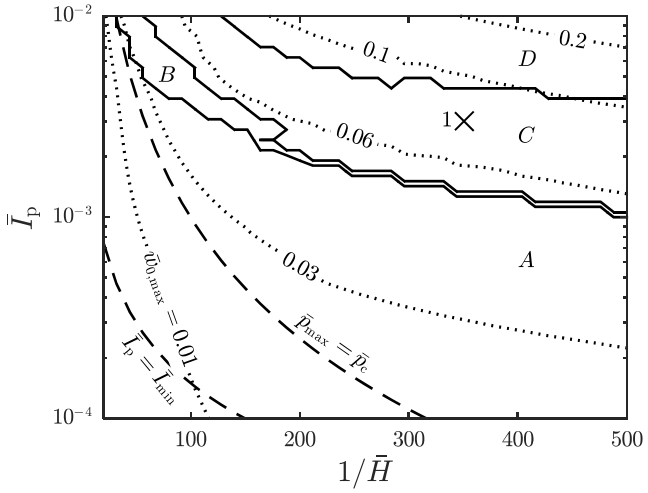

Figure 14. Regimes of behaviour and contours of maximum mid-span deflection for $\tau_\mathrm{i} = 20, \alpha_\mathrm{r} = 0.5$.